

Chapter 3

Effects of localised shearing on crystal growth and nucleation

As outlined in Chapter 1, part of the projects aim is to investigate the possibility of using optical tweezing to induce nucleation by generating fluid flow within a supersaturated solution. The intent of which would be twofold: Firstly to have a repeatable means of inducing nucleation under different solution conditions. And secondly, to understand the influence of shearing on nucleation at a micro level as compared to results in bulk fluid.

It has been shown that for macro-scale systems, the likelihood of nucleation increases to a maximum value under increased shearing [1], [2]. Mura and Zaccione developed a theoretical framework to describe how the a newly formed nucleus experiences two additional growth factors when placed in a moving fluid. Firstly, due to increased molecular transport of solute molecules the nucleation rate is enhanced in low to moderate fluid flows. But in addition, due to shear flow the crystal surface undergoes deformation which suppresses the nucleation rate undergoing faster fluid flow [2]. Experimental results with glycine solution support this theory; Debuysschere *et al* demonstrated that the nucleation rate of supersaturated glycine was enhanced up until $\dot{\gamma} \approx 3000 \text{ s}^{-1}$ [1]. After which the nucleation rate began to decrease but was still greater compared to the case where fluid flow was minimal.

Optical tweezers can been used to rotate a whole host of microscopic objects, with the fastest reported results exceeding 1000 Hz in heavy water [3]. If such a micro-rotor was suspended in a supersaturated solution the fluid flow around it could be fast enough that the nucleation rate is locally enhanced. We focused on two primary candidates for rotation, Vaterite and 4-Heptyl-4-biphenylcarbonitrile (7CB). The former being a polymorph of calcium carbonate and the latter an example of nematic liquid crystals, both of which have been used repeatedly in previous micro-rotor research [3]–[5]. In addition, we also consider the application of using techniques beam steering to generate fluid flow by trapping silica micro-beads. In this instance the fluid flow is generated not due to the transfer of angular momentum, but due to shearing caused by a moving sphere through stagnant fluid.

To begin with, the discussion of the necessary optical equipment is covered, drawing attention to specialised components and techniques that are not standard in optical trapping set ups.

3.1 Optical Tweezer Equipment

In general, all optical tweezers require a laser driver, a focusing microscope objectives, a position controller, and position detector [6]. The laser used for this project was a 1064 nm near infrared laser - provided by CNI Lasers – that was focused by a Nikon 100x oil immersion lens. The choice of an oil immersion lens is important as the optical oil used prevents a loss of focus when used on a glass cover slip. Now, experimental work has shown that the trapping efficiency increases with beam diameter up until it exceeds $\frac{2}{3}D_{obj}$ [7] where D_{obj} is the diameter of the objective aperture. To expand the beam front we utilise a Galilean beam expansion arrangement (indicated by f_1 , and f_2 in Fig. 3.1) as recommended for high power laser applications. In our initial experiments the beam expansion provides a $4\times$ magnification. Whereas in later experiments we utilised a galvano-mirror the beam expansion is $3\times$ and then the 4f correlator (see 3.1.2) provides a further $1.25\times$ magnification (using f_3 and f_4) - the magnification is

given by.

$$\frac{D_2}{D_1} = \frac{f_2}{f_1} \quad (3.1)$$

It should be noted that the galvano-mirror requires the use of a Keplerian beam expansion arrangement which reduces the transmitted laser power due to localised heating of the air. Afterwards the laser is passed through a dichroic mirror that separates incoming infrared and visible light, this is to prevent the laser from damaging the CCD camera used for imaging the trapping plane. The laser is then focused to a diffraction limited spot by the objective. Utilizing a high numerical aperture objective enhances the gradient force at the focal point; the trade-off being that the for higher NA objectives the trapping depth is reduced due to spherical aberrations. While it is possible to increase the trapping depth [8] by adjusting the objective's tube length this approach is incompatible with our trapping arrangement. A 0.25 NA condenser objective refocuses the scattered laser light and also provide an aperture for an imaging LED to illuminate the focal plane. Samples are loaded onto a piezo driven table to that is inserted between the trapping and condensing objectives; the piezo drivers allow for sub-micron control of the beam focus position to a degree as small as a 10 nm. To detect and monitor the position of a trapped particle a quadrant photo diode (QPD) was utilised.

3.1.1 Position detection methods

In order to accurately capture the dynamics of a trapped particle, a position detection system is required. There are 3 possible methods of position detection: video-analysis, lateral-effect position sensing, and photodiodes.

Video analysis is ideally suited for multiple traps or situations where precision is not the top priority. Whereas lateral-effect and photodiode position detection are two examples of back-focal plane interferometry, where the interference pattern produced by the target particle is extrapolated to determine its position. In order for video analysis to match the accuracy of back-focal plane interferometry methods requires the camera's frame rate to exceed 1 *kHz* which can be difficult to achieve while maintaining

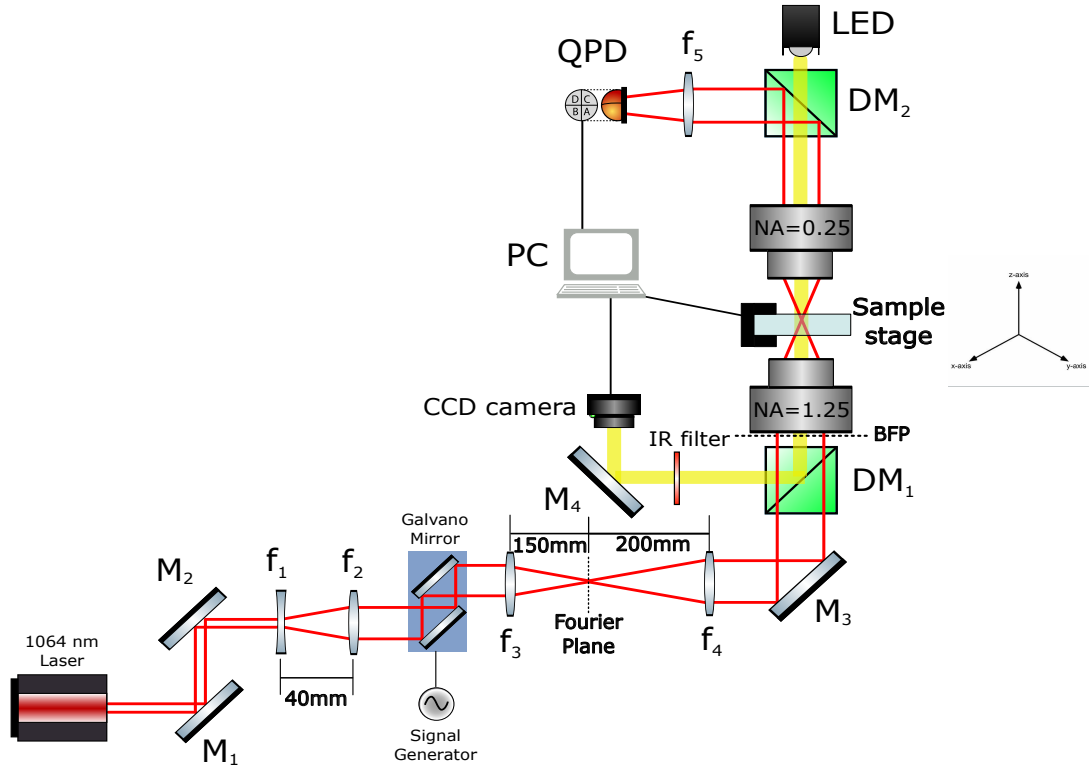


Figure 3.1: Optical tweezer set up used for the majority of the PhD. The focal lengths of f_1 , f_2 , f_3 , & f_4 are -20 mm , 60 mm , 150 mm , & 200 mm respectively [M = mirrors, DM = dichroic mirrors, f = focal lenses]. Diagram not drawn to scale.

a decent resolution [9]. In comparison off the shelf back-focal plane detectors can achieve temporal resolutions anywhere from $10 - 100\text{ kHz}$ [10].

A quadrant photo diode (QPD) is a frequently used position detection system for optical tweezers due to their high sampling rate, high degree of precision, and ease of set up. The QPD is constructed of four photo diodes assembled in a quadrant formation, when a particle is trapped the interference pattern produced is focused onto the QPD, with the maximum intensity mapping to the particle's centre of mass. By summing the voltages of the horizontal and vertical quadrants together the particle's centre of mass is tracked in the x-y plane. Axial displacement can be estimated by observing the change in the total voltage of the QPD. The outputted signal gives an indication of the particle's relative displacement from the beam focus, but in order to convert the signal to distance units the trap needs to be calibrated (assuming a linear response curve).

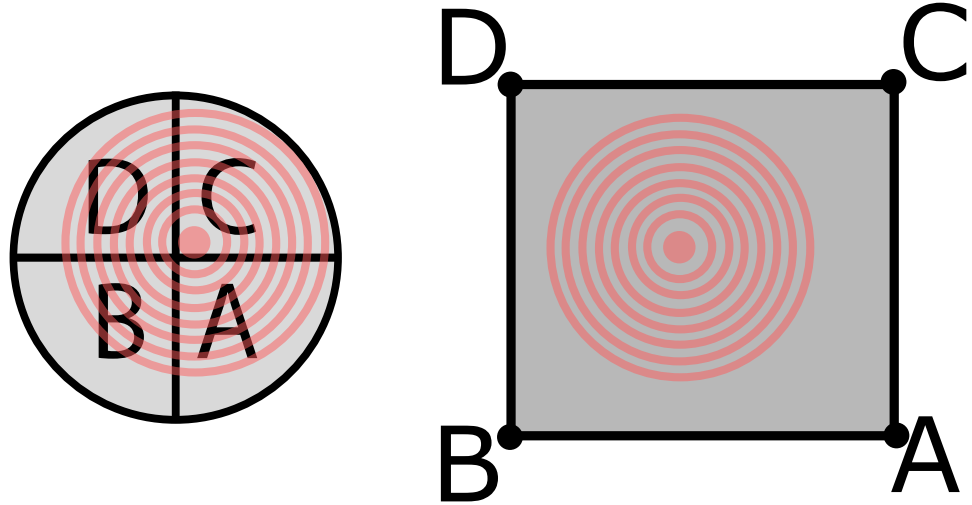


Figure 3.2: Comparison between QPD and Lateral effect photodiodes. The four quadrants of a QPD (left) experience different photocurrents based on the total intensity of light incident on each section (labelled A, B, C, D). Whereas a Lateral effect sensor (right) uses the resistive properties of the photodiode surface to vary the create different photocurrents passing through the anodes A, B, C, and D.

A lateral-effect sensor has a similar output but works using a the entire sensor as a single cell analogous to the focal plane of the trapping beam. The four corners of the sensor act as anodes connected to a base plate cathode, as the beam moves across the surface of the detector each anode will experience a different photocurrent depending on how close the centre of the interference pattern is to each anode. The advantage of a lateral effect detector is that the linear regime is much larger than a QPD making it much better for monitoring the position of a trapped particle. However, Lateral-effect sensors are often limited in their spacial resolution due to high signal-to-noise ratios, requiring a high intensity of light on the sensor in order to get a clean signal. As a result, most optical force measurements are conducted using a QPD as opposed to a lateral-effect sensor, as often the displacement is small enough that the signal-displacement

curve can be considered linear.

3.1.2 Fourier Optics and 4f correlators

As shown in 3.1, after the Galvano mirror there are a pair of focal lenses (f_3 and f_4) that do not seem to serve a clear purpose. These are in fact crucial for the operation of the Galvano, the pair of them can be more accurately called a 4f correlator.

A 4f correlator is an example of Fourier optics in practice, understanding that a focused lens takes a Fourier transform of the light profile. Consider a laser with a circular Gaussian profile, if you were to place a detector there you would pick up the intensity as a function of its position within the beam. If however you focused the light into a single point (using a +ve focal lens) you are actually seeing a measurement of the phase of your laser with position, in which you would see a diffraction limited spot ($d = \lambda/2n\sin(\theta)$), indicating that the laser is collimated. In imaging systems, a series of focal lenses can be used to filter out unwanted scattering from an image (or in an inverse case differentiate between different images), the placement of each lens is shown via fig. 3.3.

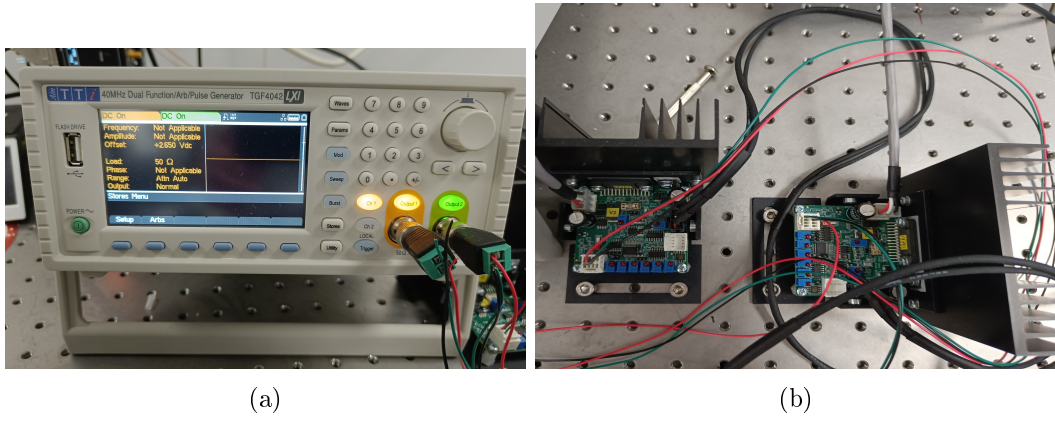


Figure 3.3: Signal generator galvano mirror controller, channel 1 controls the x-axis mirror, while channel 2 controls the y-axis mirror. Both channels can be manipulated independently.

For our applications a 4f correlator is utilised to ensure that the motion of the galvano-mirrors does not move the focal point of the laser, allowing for a stable trap even while in motion. As shown in Fig. 3.1, after the galvano-mirror we have our

two lenses - f_3 and f_4 - the former being installed 150 mm from the second mirror of the galvano, and the latter being installed 200 mm from the back focal plane of the trapping objective. The signal generator used was supplied by 'MCS Test Equipment Ltd', allowing for dual channel signal control. This allowed us to precisely control the alignment, amplitude, phase, and frequency of both mirrors making alignment much easier.

While in theory the frequency can be increased until the mechanical limit of the mirrors is reached ($\approx 1000\ Hz$), the practical upper limit is determined by the trap strength. For a silica sphere this is on the order of 300 Hz when suspended in water. Likewise while in theory the signal amplitude can be increased until the voltage limit of the motors is reached ($\approx 5.0V$) the geometry of the focal lenses limits the maximum amplitude to 0.5V as any greater will move the laser beyond the lens. For basic trapping calibration the galvano-mirrors were set to DC output, providing a fixed spot which operates like a typical optical trap.

3.2 Synthesis of Birefringent Micro spheres

There are several options for particles that can be rotated using optical tweezers [4], [5]. Over the course of the project two different micro spheres where investigated, Vaterite and liquid crystal droplets. Both can be readily synthesised in the lab and are will rotate at a variety of sizes (see ??).

Vaterite is a polymorph of calcium carbonate that is rarely seen in nature due to its low stability [11]. All three polymorphs are inherently birefringent meaning that they can be rotated using circularly polarised light. However unlike its other polymorphs of calcite and aragonite, when synthesised vaterite will typically form small spherical particles making them ideal for optical trapping and rotation. Synthesis of Vaterite micro spheres requires fine control of the crystal growth process in order to maintain polymorphic stability. Though for the purposes of optical rotation the exact polymorph is not as important as its morphology as all 3 polymorphs are inherently birefringent.

Vaterite samples where made by the first preparing equal amounts of $CaCl_2$ and

Na_2CO_3 at a concentration of $0.33M$, at the same time a vial of $0.33M$ $MgSO_4$ was prepared and set aside for later. First a small vial was filled with $1.5mL$ of $CaCl_2$ followed by $60\mu L$ and $90\mu L$ of $MgSO_4$ and $NaCO_3$ respectively, forming a seed solution. Next, a larger vial was filled with 5 mL , 1.5 mL , and 1 mL of $CaCl_2$, $MgSO_4$, and $NaCO_3$ respectively followed by the seed solution. After 10 minutes of slow but continuous mixing a few drops of Agepon was added to halt the reaction, the solution was filtered and washed 3 times with distilled water before being suspended in water.

When trapped in circularly polarised light, the anisotropic crystal lattice allows spin angular momentum to be transferred to the Vaterite particle, resulting in a rotation about the beam axis. Because the particle scatters light anisotropically the signal detected by the QPD shows periodic fluctuations [12]. In addition due to the change in polarisation there is also a periodic variation that appears at twice the rotational frequency [13]. Therefore, the resulting power spectrum is not a Lorentzian but now also displays peaks that appear at integer multiples of the particles rotational frequency.

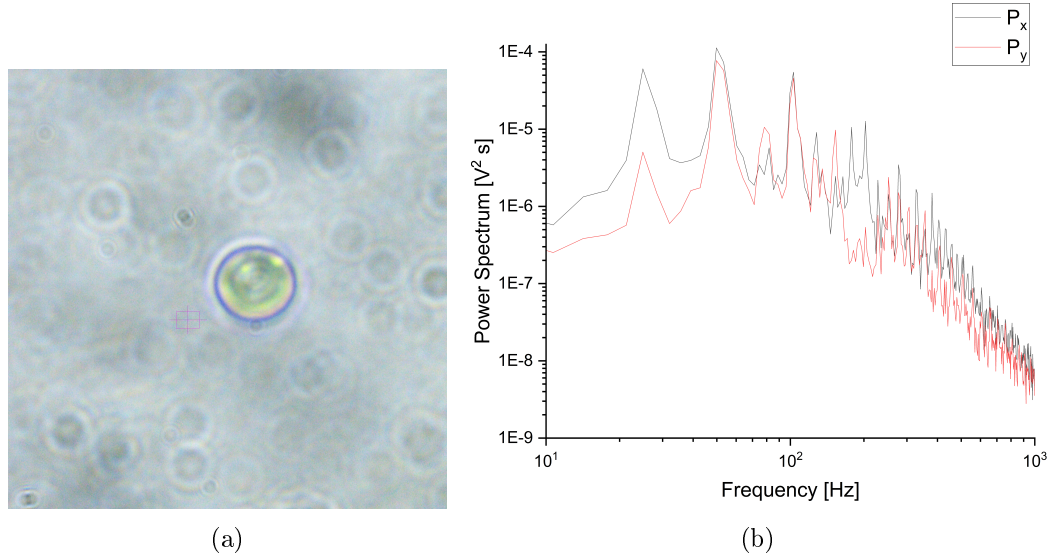


Figure 3.4: (a) Sample Vaterite sphere suspended in water and trapped by circular polarised trap. (b) Collected power spectrum from rotating Vaterite, peaks in the power spectrum appear at integer multiples of the rotational frequency ($f_{rot} \approx 49.8\text{ Hz}$)

As shown by Fig. 3.4(b) the power spectra produced still demonstrates a Lorentzian

curve but modified with these periodic peaks, while the Lorentzian can be loosely fitted to the end tail there exists no current model for describing the power spectra. The closest approximation to this was conducted by [12] where they describe the rotational motion of ellipsoidal polystyrene particles. The critical assumption being that the particle perfectly rotates in the $x - y$ plane. It has long been suspected that birefringent microspheres experience torques outside of the $x - y$ plane [14] making it very difficult to characterise the behaviour of rotating birefringent microspheres without a proper understanding of the full optical torque being applied to it.

3.2.1 Liquid Crystal Rotors

Liquid crystals are an intriguing example of materials with mixed phase properties. Unlike typical solutes such as Glycine, a liquid crystal can still maintain some degree of order between its individual molecules while in the liquid state. This is due to the fact that liquid crystals are constructed of ordered molecules that demonstrate a long range ordering. There are three main types of liquid crystal transition methods: Thermotropic crystals will transition to their liquid crystal phase when sufficiently heated. Lyotropic materials can undergo this transition due to changes in temperature and concentration. And lastly, Metallotropic materials - which are composed of both organic and inorganic molecules - change phase according to the ratio of organic to inorganic molecules present. Liquid crystal rotors are rather simple in their production, 4-Heptyl-4-biphenylcarbonitrile (7CB) was purchased from Sigma Aldrich and a small amount was added to a vial of distilled water. The solution was then heated in a water bath to 25° in order to transition the solid crystal into its liquid crystal state. The solution can then be loaded onto a sample cover slip and the individual droplets visualised. The molecules of 7CB will align with a strong electric field, and due to the spherical droplet geometry the droplets are inherently birefringent.

The liquid crystal droplets had a much faster rotation rate than comparable Vaterite spheres, due to their higher degree of birefringence and the fact that the droplets are far closer to perfect spheres making angular momentum transfer more efficient.

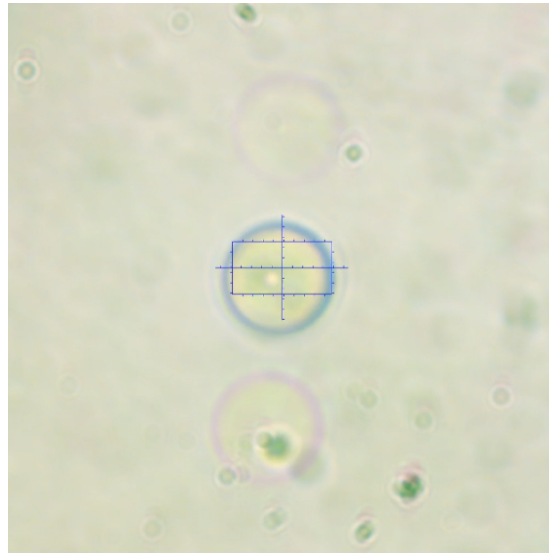


Figure 3.5: Liquid crystal undergoing rotation due to the circularly polarised trap.

3.3 Rotation of birefringent micro spheres

Optical tweezing has often been used for micro-rheology, by computing the exact forces being exerted on the trapped sphere, one can determine the local temperature/viscosity of the medium [15], [16]. When it comes to optical rotation, a rotating particle will experience a fluid drag torque that is proportional to its rotation rate, the maximum rotation rate is when the fluid drag is equal to the optical torque of the laser [16]. Optical rotors have been used to measure local temperature changes [15], or for understanding how fluid shear propagates through a medium [17]. Likewise, one can use a beam steering arrangement to probe the drag force of the fluid, by understanding the trap strength (calibrating using a low frequency signal) one can measure the drag force experienced by the local fluid [18]. I

For any discussion of fluid flow its important that we know the fluid regime which is given by the Reynolds number. For a sphere submersed in a moving fluid of velocity U this is given by:

$$Re = \frac{\rho U D}{\mu} \quad (3.2)$$

Where D is the sphere's diameter, and ρ and μ are the fluid's density and viscosity

respectively. In our case we do not have a fluid moving around a sphere but a sphere moving through the fluid at some velocity U , assuming a no-slip boundary condition we can model the fluid velocity profile based on the velocity of the particle. Assuming that for now the fluid properties are unaffected by the rotating particle we see that for an individual sphere the Reynolds number can only change due to increasing/decreasing the fluid velocity. The fluid velocity is directly proportional to the particles rotation rate for low Reynolds numbers [19]. Given the small size of the particles used ($1 - 10\mu m$ in diameter), and the relatively low rotation rates that are possible with an optical tweezer, for the case of our analysis the Reynolds number will not never be large enough to consider factors such as turbulence. There are two possible avenues for generating shear flow with a trapped particle; rotation of birefringent particles, and fluid flow induced by particle motion.

Rotating birefringent particles are the more common method for generating and measuring fluid flow in a solution. To see if we can even achieve the theoretical maximum shear rate, Vaterite spheres were synthesised (see Sec.3.2) submerged in water and trapped with the 1064 nm laser at set to 450 mW. The rotation frequency was determined using the QPD, and the particle sizes were computed by image analysis. With the particle size and rotation frequency, the tangential rotation speed is calculated via:

$$u(r) = \frac{\pi}{4} \frac{d^3}{r^2} \omega \quad (3.3)$$

Where d is the particle diameter, ω is the rotation frequency reported by the QPD, and r is the distance from the particle's centre. Using Eq.3.3 we calculated the fluid flow radiating outward from the centre of the sphere. The shear rate can then be computed as the partial derivative fluid flow (assuming shearing is generated purely by the flow field). This approach was used previously with liquid crystal rotors [4]:

$$\dot{\gamma}(r) = \left| \frac{\delta u(r)}{\delta r} \right| = \frac{\pi}{2} \frac{d^3}{r^3} \omega \quad (3.4)$$

One would expect that we set some reference distance where the fluid flow would be considered zero. However, at a microscopic level we are more concerned by the

fluid shear for an individual nucleation event. We are essentially computing what the shear rate would be for a small volume of fluid between two moving parallel plates. This is similar logic to Mura and Zaccone's work where they considered the shear on a subcritical nucleus in a flow field [2]. They go further in depth to discuss the impact of material transport, overall coming to the conclusion that increasing shear rate leads to an increase the nucleation rate up till some maximum.

3.3.1 Estimation of fluid flow around a rotating particle in bulk fluid

First we determined the upper rotation rate that could be achieved using both Vaterite and liquid crystal spheres. Vaterite samples were synthesised according to [5], [20] (see sec. 3.2), and then suspended in distilled water. A sample of $200 \mu L$ was pipetted and a single microsphere was captured via a circular polarised beam.

Due to Van der Waal's forces some of the microspheres were stuck together, fortunately individual sphere's were still present. Individual microspheres were trapped and their rotation rate was determined by looking at the peak frequency component of the collected power spectrum. Due to their anisotropic scattering the QPD signal will oscillate periodically. After taking the Fourier transform of the QPD signal the power spectrum has distinctive peaks at integer multiples of the rotational frequency. The largest peak is often twice the rotational frequency which is due to the polarization modulation of the scattered field, the first peak is due purely to the rotation of vaterite sphere [13]. An example of this behaviour is shown in fig. 3.6.

The accuracy of the rotational frequency is dependent on the sample rate of the QPD and the sample duration [10]. With higher sampling rates resulting in a wider frequency window (see Sec.??) and longer sampling durations resulting in more distinct rotational peaks. The default QPD sampling rate is $2^{17} Hz$ which is more than adequate for detecting even the slightest low frequency signals. And the default sampling duration was $3 s$ which for most cases gave us clear distinct peaks for even relatively low rotational frequencies. After trapping a vaterite microsphere the power spectrum was recorded and the rotation frequency was acquired. This was repeated several times for each sphere trapped, to confirm that the rotational frequency was constant and that the sphere had

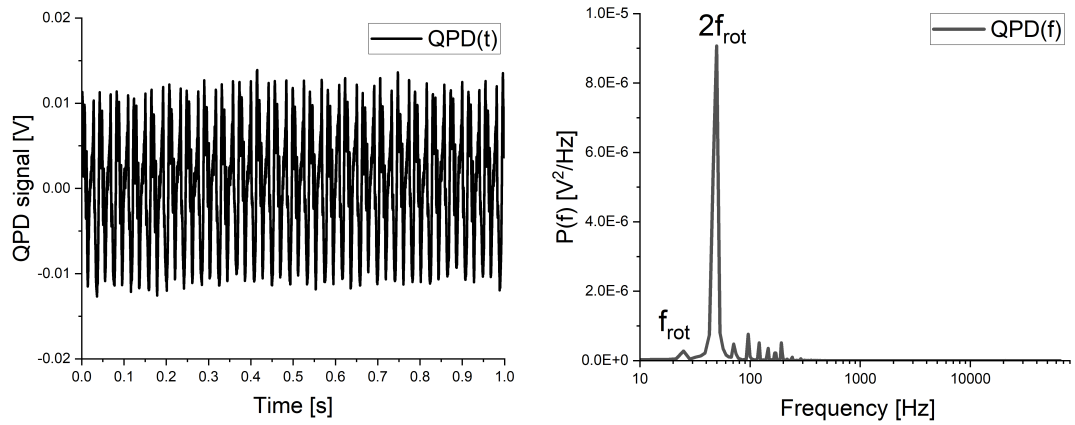


Figure 3.6: Example of QPD signal being converted from the time domain to the frequency domain. (left) Raw signal collected from the QPD over the 1st second of its trajectory showing a periodic spacing with a period of $1/f_{\text{rot}}$. (right) Power spectrum of the QPD signal, the y-axis is a linear scale to demonstrate the clear peaks in the power spectra. The rotational frequency is the first instance of a peak forming, and after that the peaks appear in integer multiples of f_{rot}

reached its maximum rotation rate.

After computing the rotational frequency the radial fluid speed could be estimated using Eq. (3.3). From there we can estimate the shear flow experienced by a small volume of fluid within the flow field (see Eq.(3.4)). Here we only consider the fluid flow as it propagates outward from the axis of rotation. While the cover slip will have some effect fluid flow it is difficult to quantify the effects of a hard boundary on a rotating object when the boundary is perpendicular to the axis of rotation.

From Fig.3.7 there is not a strong relationship between particle size and rotation rate, this is contrary to much of the theoretical predictions that predict an exponential decay with particle size. This can be in part due to the fact that synthesising perfectly spherical spheres that have uniform birefringence across the whole population is difficult. Despite our best efforts at controlling the growth rate the smallest particle ever synthesised was around $3 \mu\text{m}$ in diameter. The Vaterite spheres would often stick together while suspended in water after a short period of time. The fastest reported rotation rate within a fluid was by [3] that achieved a rotation rate of 5 kHz , this is plotted in Fig 3.7. In addition we added the results from [5] as a more realistic example.

The optimal shear rate predicted by [1] is plotted on Fig. 3.7(b), the outer dotted

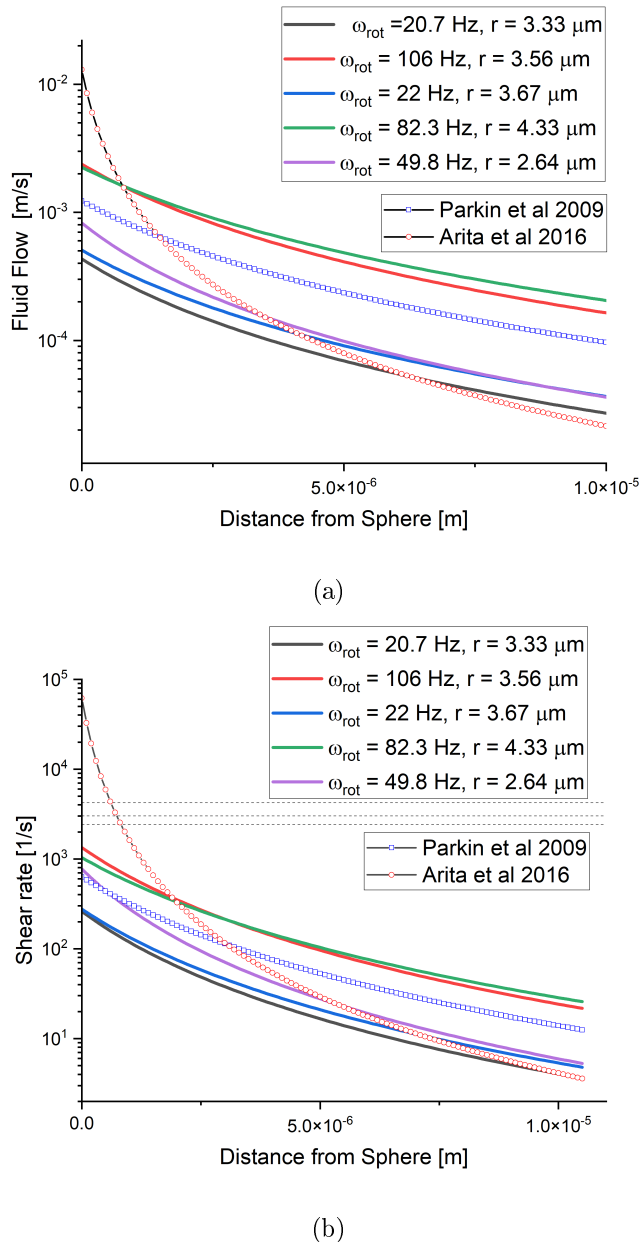


Figure 3.7: (Top) Fluid flow radiating out from the surface of a rotating Vaterite sphere. (Bottom) Shear rates computed using Eq.3.4, optimal shear rate is of 3000 s^{-1} is indicated by the dotted line. Vaterite radii and rotation frequencies are shown, the laser power was kept constant at 450 mW. Reported rotation rates, and their corresponding fluid flow and shear rates, for Vaterite are also plotted alongside lab results. Results from [3], [5] are included as well.

lines represent the point when the nucleation rate is less than 90% of the maximum. We can visualise the fluid around the rotating sphere by dividing it up into radial sections. Assuming the sphere is rotating sufficiently quickly there are three sections of concern, as demonstrated by fig. 3.8. The fluid close to the sphere experiences a shear rate that is far greater than the optimal shear rate, in which case nucleation is suppressed [2]. Secondly, there is a region of fluid that experiences a shear rate close to the optimal value ($\pm 5\%$) where the nucleation rate is enhanced significantly compared to the bulk fluid. Lastly, beyond the optimal region the shear rate drops off exponentially in which case the nucleation rate is barely different compared to the bulk fluid.

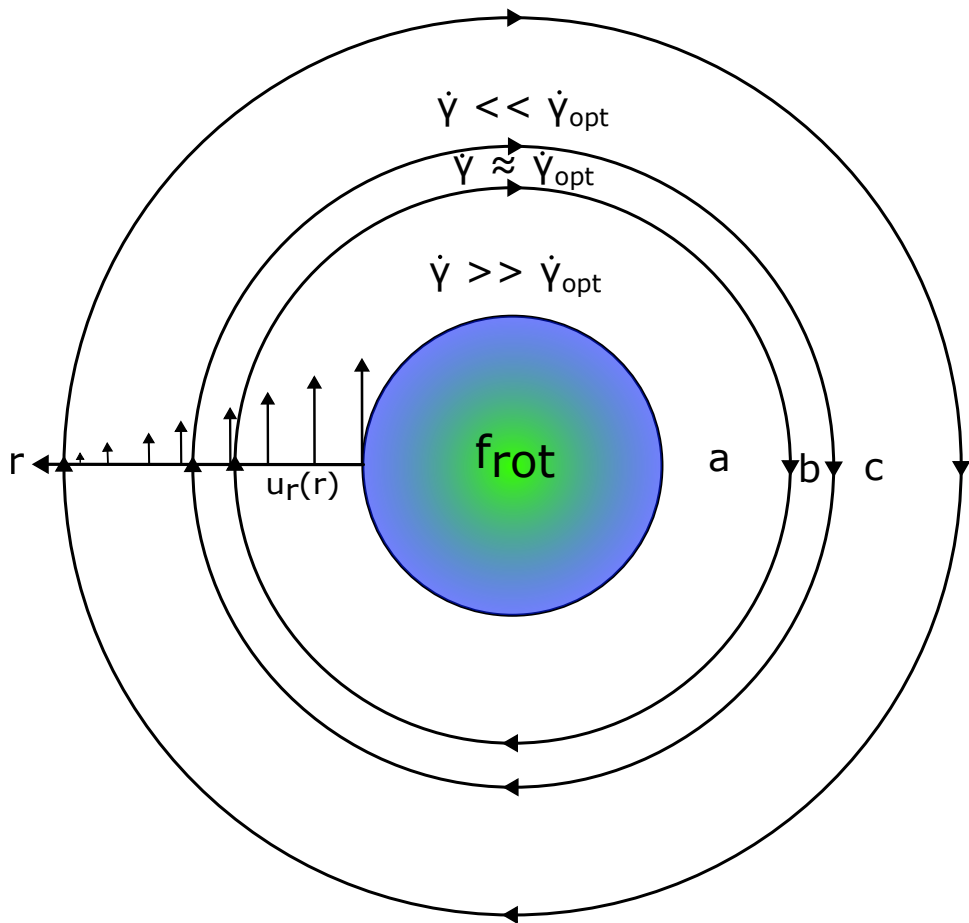


Figure 3.8: Diagram demonstrating how fluid shear rate varies radially from a rotating sphere (rotation rate = f_{rot}). (a) the shear rate exceeds the optimal shear rate ($\dot{\gamma}_{opt}$) and suppresses the nucleation rate. (b) shear rate is close to the optimal amount, enhancing the nucleation rate. (c) shear rate is far below the optimal amount and the nucleation rate is comparable to the bulk fluid.

3.4 Rotating spheres in Supersaturated solution

If rotation rates in bulk solution are insufficient then a rotating sphere close to an artificial barrier may be able to improve the shear rate of the surrounding fluid. Of course placing a solid barrier in a supersaturated fluid may well encourage nucleation somewhere on the surface outside of our control. Instead we chose to use the droplet edge of the supersaturated solution, while not a hard barrier per say, the molecular mobility close to the droplet edge is reduced due to surface tension. Furthermore, it has been shown through multiple results that nucleation is enhanced at the air-solution interface [21]–[23].

Estimating the distance from the trap focus to the cover slip is difficult to measure directly, often requiring one fits a complex Lorentzian curve to the recorded power spectra in order to measure the fluid drag from being in close proximity to the cover slip [10]. We estimate that the vaterite must be at least $15 - 20\mu m$ from the cover slip for us to reliably trap them. The contact angle between the cover slip and solution was previously measured in [24], while being loosely dependent on the supersaturation the measured contact angle for supersaturated solutions was between 30° and 35° . This is shown in fig.3.9.

Supersaturated solutions of glycine and water were prepared and stored in an incubator at $40^\circ C$ prior to use. When ready to be studied $15 \mu L$ of vaterite suspension was pipetted into the solution and $20 \mu L$ of the combined solution was pipetted onto the cover slip. A Vaterite sphere was located, trapped, and moved to the droplet edge where the solution meets the cover slip. This removed the need for hydrophilic coatings to achieve a flat fluid layer (as used by [21], [25]).

Particle sizing was achieved by converting the particle diameter from pixels to physical units within an accuracy of $\pm 0.05\mu m$. The QPD was used to measure the frequency of fluctuations in the QPD signal. After measuring the rotational frequency the sphere was left to rotate for a period of ten minutes after which, if no nucleation event was observed the particle was released. The overall results are catalogued in table 3.1.

It should be noted that rotational frequencies equal to $0.00 Hz$ are not due to

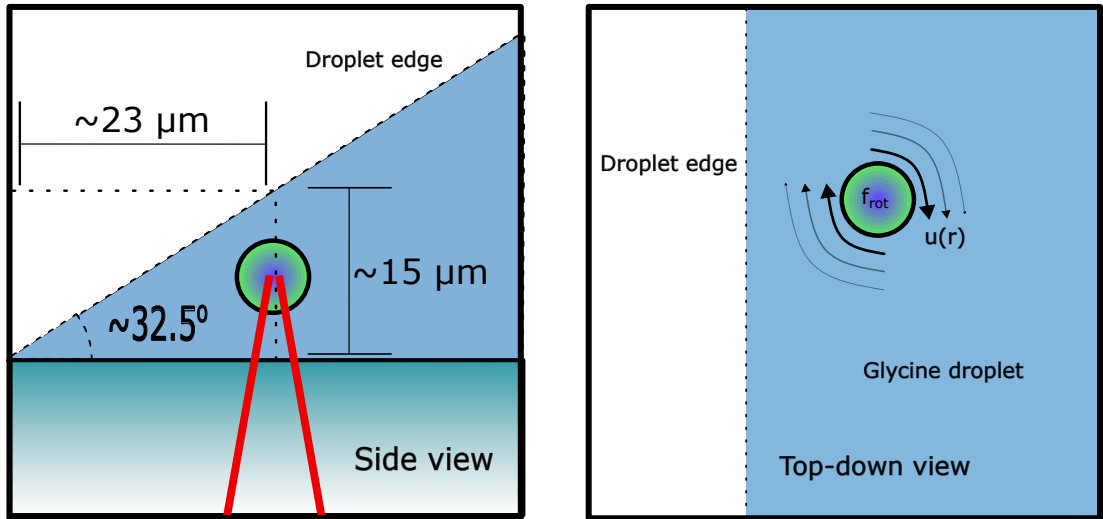


Figure 3.9: Diagram of optical trapping set up for rotating birefringent particles in a supersaturated solution. Left: side view of the trapping set up showing the location of the trap focus at the edge of the droplet of a supersaturated solution. The approximate contact angle (calculated by [24]) is used to provide a scale of how close a trapped particle could be located. Right: top down view of the glycine droplet with a trapped birefringent particle shown close to edge of the trap. As the particle rotates the drag force from the surrounding fluid generates a flow field around itself (see Eq. 3.3).

Table 3.1: Results from rotating Vaterite within supersaturated solution of H_2O and Glycine. Solubility concentration for Glycine at 16° was $C^* = 0.2016g/g$

| Super Saturation | Particle radius [μm] | ω [Hz] | Nucleation [✓/✗] |
|------------------|-----------------------------|---------------|------------------|
| 1.01 | 2.34 | 10.4 | ✗ |
| | 3.26 | 8.46 | ✗ |
| | 5.67 | 9.63 | ✗ |
| 1.14 | 1.89 | 1.23 | ✗ |
| | 3.75 | 3.54 | ✗ |
| | 4.35 | 4.86 | ✗ |
| 1.4 | 1.59 | 0.00 | ✗ |
| | 3.47 | 0.00 | ✗ |
| | 6.24 | 0.00 | ✗ |
| 1.45 | 3.68 | 0.00 | ✗ |
| | 5.43 | 0.00 | ✗ |
| | 6.32 | 0.00 | ✗ |
| 1.49 | 1.52 | 0.00 | ✗ |
| | 4.76 | 0.00 | ✗ |
| | 7.27 | 0.00 | ✗ |

a rounding error. Simply looking at the live video shows no rotation of the vaterite particles, and even looking at the QPD signals shows no discernable fluctuations that would arise due to rotation. Trying to trap a particle close to the edge proved more challenging than expected. Unlike in previous reports where the beam is focused at the upper edge of the droplet [21], [22], [26], we attempted trapping in close to the contact point of the droplet and the cover slip.

It is suspected that trapping is much harder at the interface due to increased surface tension and unpredictable scattering forces. The closest we could trap a microsphere to the droplet edge was in the range of $5 - 10\mu m$, at that distance the fluid flow is so low that even the presence of a hard boundary would be insufficient for shearing the fluid. Furthermore, as is evident in Table 3.1, the rotation rate drops off significantly with increased supersaturation, due to higher fluid viscosities. While in theory a sufficiently focused laser could rotate any microsphere to a fast enough to reach the shear rate predicted by [1] the localised intensity would be so large that even using D_2O would see a significant increase in temperature.

It is not impossible that fluid shearing could be used in the future to localise nucleation; but from these results, using individual micro-rotors is not an appropriate method due to two key factors. Firstly, the area of influence is far too small to see any noticeable increase in the nucleation rate this is demonstrated most clearly in fig. 3.7. Due to the exponential decay in the expected shear rate it is very difficult trying to shear a large volume of fluid. Even if the optimal shear rate at a micro-level was an order of magnitude less than what was predicted by [1], only a small volume of fluid would even experience that shear rate. In order to properly understand the microscopic effects of fluid shear a method of localised shearing over a larger fluid volume is necessary.

Secondly, increased fluid viscosity significantly reduces the limits the maximum rotation rate possible. As indicated by 3.1, the rotation rate achievable by a vaterite sphere falls off significantly with increasing supersaturation. Experimental estimations of relative viscosities showed a 12% increase when looking at undersaturated glycine solutions ($S \approx 0.34$) [27]. As far as we are aware there are no reported fluid viscosities for higher supersaturations. Extrapolating the results from [27] suggests that a saturated

solution would have a 35% increase in fluid viscosity (compared to pure water). This also does not account for any other factors such as the fact that close to a boundary a rotating particle will experience a reaction torque from the stationary surface [19].

If multiple micro-rotors could be trapped in close proximity to one another they could create a large region of fluid where nucleation is more likely than the bulk fluid. Because optical torque is not contingent on the fluid properties the only limiting factor would be the total angular momentum transferred to each particle. Micro-rotors have been created that allow for precise control of suspended micro-particles [28] and could potentially be used to generate sufficient shearing. However these could not be used in this project as we lacked the necessary hardware to form multiple gradient traps.

3.5 Nucleation with a Stationary and Moving Beam

As mentioned previously, shearing via optical rotation did not result in any localised nucleation events even while in the proximity of the droplet edge. An alternative approach was suggested, using a galvano mirror to move a particle quickly through a supersaturated solution. Preliminary calculations suggested a particle moving rapidly through a fluid could produce significantly greater shear rates (see *Appendix X.X* for breakdown) than a rotating particle. While a particle is within the optical trap the gradient forces are significantly reduced meaning simply trapping a particle is insufficient for inducing nucleation [24]. This is why we did not see any nucleation events while rotating the vaterite, there is not a large gradient force to draw in material.

During initial testing using silica beads we found that even in undersaturated solutions the optical trap would produce a crystal nucleus when the trap was empty. This has been reported prior [21], [25], but what is more interesting is how the beam's motion influenced the growth of the nucleus.

3.5.0.1 Choice of Crystal growth rate units

The growth rate of a crystal can be described using different units depending on the situation. For example, seed crystals often use growth units in the form of *length per*

unit time. This can either be used to describe the overall length of the longest edge of a crystal, or to describe how individual faces grow separately. This works well for crystals with a clear morphology, in regards to laser induced nucleation the crystal growth is heavily influenced by the local fluid conditions meaning tracking the length of an individual face is challenging. Instead we utilise image analysis software such as imageJ to measure the area of the crystal after each frame to get a rough estimate of the crystal growth rate in units of *length² per unit time*. With the addition of the contact angle information from [24] we can approximate the crystal height based on how close it is to the droplet edge.

3.5.1 Stationary beam

Its well known that a supersaturated solution can nucleate if irradiated by a focused beam with sufficient power [25]. First we look at how a laser induced nucleation event unfolds using a stationary focused beam. The laser was focused at the edge of a $20\mu L$ droplet consisting of water and dissolved glycine ($S = 1.03$). The solution was monitored for 10 minutes, if a nucleation event was observed the event was recorded using a high speed CCD. If no nucleation event was observed after 10 minutes the solution was disposed of and a new sample was prepared. After ten repeats only 30% of the samples observed a nucleation event at the focus. All of which displayed similar growth behaviour to one another.

Consider Fig. 3.10, the frames taken from a nucleation event, the beam is a stationary being $\approx 3.5\mu m$ from the droplet edge. After a period of roughly 5 minutes a nucleus forms at the trap focus, growing quickly (growth rate was approximated using imageJ to be on the order of $700 \mu m^2/min$) from the focal point of the trap until after roughly 6 seconds the crystal escapes. A likely reason that the trap is escaped is due to the fact that crystal is far too large to be held in place and is in fact still growing as the solution is supersaturated. Based on the contact angle measurements from [24], the droplet height could not have been any more than $2 - 5\mu m$ at the trap focus.

Comparing to previous literature using optical tweezers shows that the growth rate is only loosely connected to the solutions supersaturation. Crystal growth rates for a so-

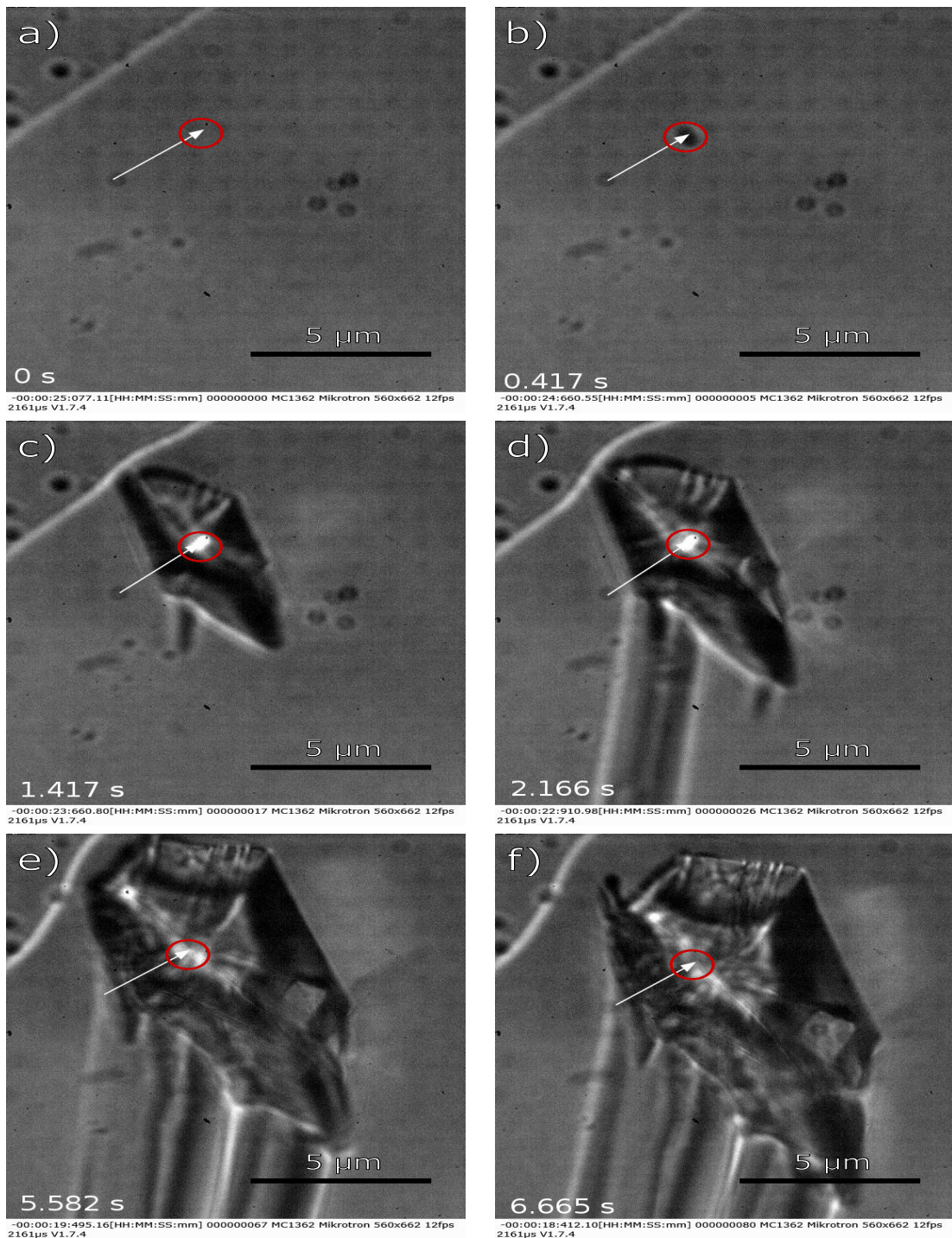


Figure 3.10: Laser induced nucleation at the edge of a droplet of supersaturated glycine solution. (b) shows the first instance of a crystal nucleus, growing quickly through (c)-(e) until after 6.665 s the crystal begins to escape the trap.

lution of glycine and water ($S \approx 1.00$) was found to vary from as much as $3900 \mu m^2/min$ to as low as $675 \mu m^2/min$ [24]. The reason for such high crystal growth rates is due primarily to the tweezer focus bringing in material due to gradient forces. A study of glycine crystals in water found that for a similarly supersaturated solution the growth rate along the 011 face was around $0.1 \mu m/min$ where as the 010 face was found to have a growth rate of around $0.01 \mu m/min$. While its difficult to extrapolate an exact area growth rate from these results we can approximate that if the we looked directly perpendicular to the crystal growth the area would increase at $\approx 0.02 \mu^2/min$ (see X.X for a breakdown of this approximation).

The key take away to remember is that the beam has no influence over the crystal shape, instead it grows outward from the trap focus. Furthermore, due to the fact that the solution is supersaturated the crystal growth cannot be contained to the trap focus. Instead the crystal escapes as its size exceeds the trap focus.

3.5.2 Moving Beam

To test if a rapidly moving silica bead could generate the necessary shear rate for crystal nucleation we wanted to see if a trapped silica bead could be trapped and moved in an aqueous solution. $20 \mu L$ of glycine and water ($S = 1.03$) was added to $10 \mu L$ of a dilute water-silica mixture making the solution unsaturated ($S \approx 0.7$). However, due to the beam's motion we instead encountered unexpected growth behaviour.

Shown below in Fig. 3.11 where we have the laser focus moving in a small elliptical pattern. While nothing is seen directly entering the focus a nucleus forms close to the droplet edge, unlike in fig. 3.10 the crystal does not grow out from the focal point evenly. Due to the galvano mirror, the crystal is simultaneously being moved by and growing around the focal point of the trap. Because of this the crystal nucleus lacks a clear morphology at first. Until roughly $20 s$ the crystal reaches a almost prismatic structure, with further irradiation increasing the size.

Interestingly the galvano-mirror allows the trap to impart a slight torque on the crystal, as shown in fig. 3.11(c) and (d), where even though the crystal is not directly in the trap focus it rotates in the $x - y$ plane and gets trapped again at a corner. The

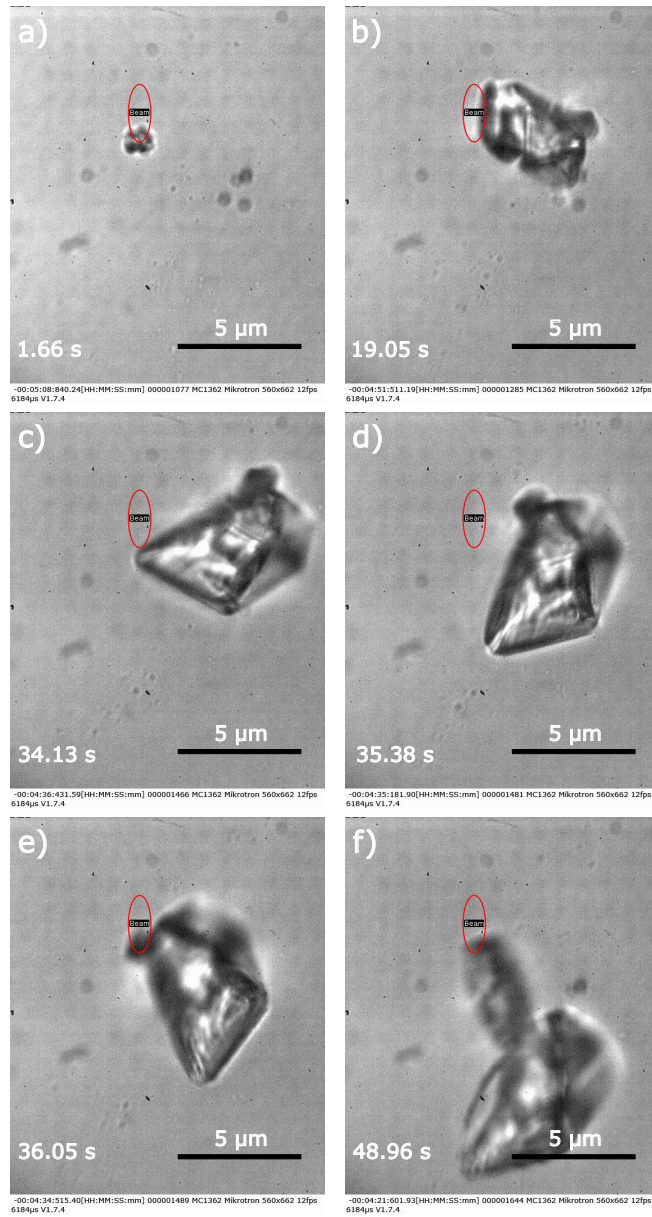


Figure 3.11: Frames from a longer video depicting the growth of a nucleus using a moving beam. Beam power is kept at 700 mW and the supersaturation was estimated at $S=0.86$. Initially the crystal shape is amorphous (a) but eventually reaches a more regular shape (b). This crystal is still influenced by the optical trap as even when not directly irradiated by the laser the crystal rotates between (c) and (d). When the laser is focused on a corner the crystal growth is localised to that region, resulting in an elongated section forming between frames (e) and (f).

rotation could not be due to fluid flow close to the surface of the crystal as the dipole moment of individual water molecules is too small to be influenced by an optical trap. In figs.3.11(e) and (f), the crystal growth becomes localised to the corner. The area growth rate between figures 3.11 (a) and (d) was approximated using imageJ at $45.03 \mu\text{m}^2/\text{min}$, whereas between figures 3.11(e) and (f) the growth rate at that particular edge was estimated at $42.10 \mu\text{m}^2/\text{min}$.

Nucleation in undersaturated conditions has been reported previously in D_2O [25] and H_2O [24], though not involving a moving beam. This modification allows for the crystal growth to be localised to a specific region of the bulk crystal whereas with a stationary beam there is no control over the crystal morphology. In fact this allows for a much finer control over the exact shape of the crystal nucleus, in some cases allowing for growth out of the viewing plane as shown in fig. 3.12.

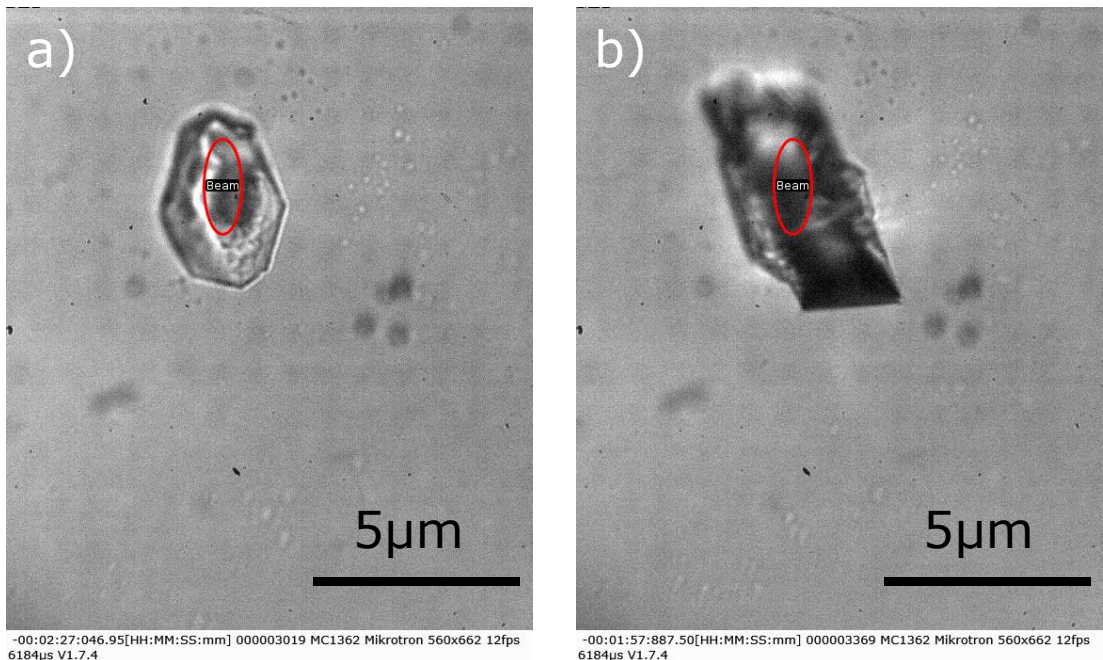


Figure 3.12: Interesting crystal growth on the surface of an existing crystal. Initially the crystal surface seems flat (a) but eventually a different crystal structure grows out off the surface (b).

Where a large outgrowth forms on the surface of a nucleus, over a period of 30 s the outgrowth develops into a rhombic crystal structure. The unique crystal growth

demonstrated is likely a factor of the moving beam focus, but this raises a question over how the laser can localise the growth only around the focus and why the crystal does not grow or shrink when not directly within the trap. There should be some material that is being drawn into the trap as it scans across the camera frame.

3.5.3 Direct trapping of Glycine clusters

In a repeat experiment a solution similar to sec. 3.5.1 was made up, but without any silica micro-spheres. Once again the beam was focused close to the droplet edge, this time the galvano mirror was scanning a circular path (as shown in fig. 3.13). After a few minutes of irradiation droplets were seen entering the camera frame. Because no silica had been added, and that the solutions were filtered, these droplets had to be from the glycine solution. Trapping individual droplets did not result in immediate nucleation even after several minutes being trapped. Trying to bring two droplets together resulted in nucleation between the two droplets, compared to 3.5.1 & 3.5.2 the growth is much slower, taking nearly 40 seconds before the crystal structure becomes clearer.

The fact that these droplets can be trapped indicates they must have a higher refractive index than the surrounding solution. Previous reports have shown that a focused trap will draw in solute material from the bulk [29], [30]. This suggests that the droplets observed are concentrated spheres of glycine, which also explains how nucleation was initiated when those two spheres were brought into contact with one another. The droplets must be providing material for the crystal growth. It has been shown that the concentration of glycine solution is correlated with the refractive indices of the liquid [30], [31]. This suggests that we could measure the concentration of individual droplets based on the trapping strength of each droplet.

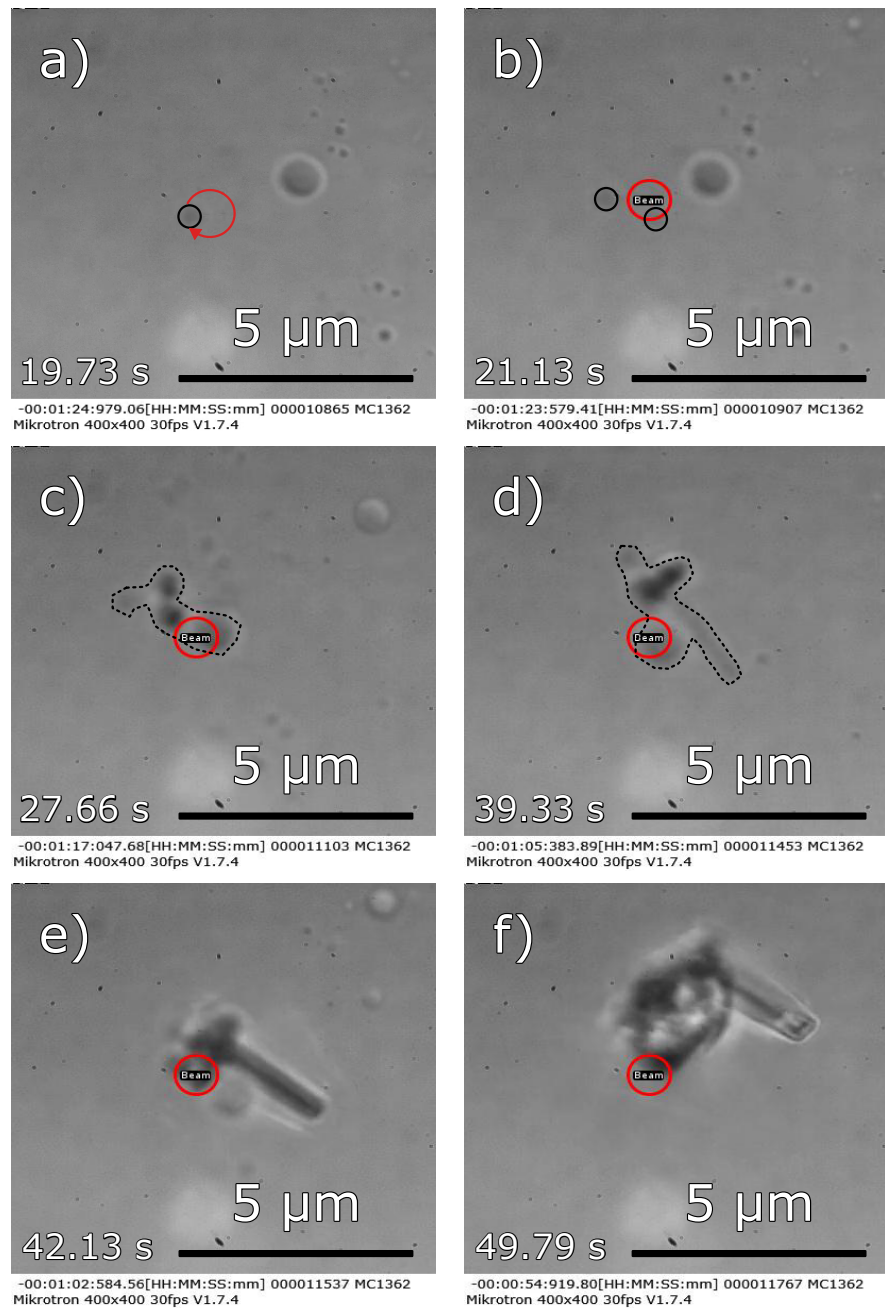


Figure 3.13: Frames from a longer video demonstrating the trapping of a glycine droplet. Solution is undersaturated glycine and water ($S = 0.86$), with the laser power set at 750 mW. (a) shows a trapped droplet (outlined in black) being brought into contact with a larger droplet. (b) upon contact a nucleus can be seen between the two droplets. The growth is rather slow with the crystal having no clear defined morphology through (c) and (d). Between frames (e) and (f) the larger droplet finally joins the main crystal.

3.5.4 Influence of a moving beam front on seed crystals

One potential application of this phenomena would be in using a moving the moving beam front as a method for shaping the final crystal morphology. Therefore, we wanted to test if a moving beam front could have any influence on the shape of a seed crystal submerged in a bulk solution. Glycine seed crystals were grown via evaporative crystallisation over night. The resultant crystals were as wide as 0.5mm in some cases. Individual crystals were collected and suspended in a water + glycine solution ($S = 1.001$) and the laser was scanned along a narrow linear path. It should be noted that the seed crystal was fully submerged in the solution, meaning that there is no interface between the air and solution close to the seed. Five separate repeats were conducted, all demonstrating similar behaviour to one another.

As shown by fig. 3.14 the laser does not in fact promote crystal growth but instead forces the crystal to dissolve into the bulk solution. The dissolution rate is not as substantial as the growth rate seen in previous sections. It takes over 20 minutes for the for the crystal surface to dissolve more than a few microns. Furthermore we do not report any sightings of droplets close to the surface of the crystal nor do we see anything enter the optical trap.

This has some implications: Firstly, the lack of supposed glycine droplets suggests that the presence of an interface is crucial in order to promote the formation of these droplets. This is consistent with previous reports on laser nucleation, where a air-solution or solution-glass interface is necessary for the trap focus to have any noticeable effect on the solute [21], [25], [30]. Secondly, the fact that the seed crystal dissolved in a saturated solution suggests that this could be due to a localised heating effect. A commonly used heating model for optical tweezers is the Peterman model [32] which accounts for the lateral distance between the optical trap and a local heat sink (such as the glass cover slip or microscope objective). Even with the heat sink the predicted temperature rise in pure water would be around $5 - 10K$. The fact that the seed crystal dissolves so slowly could simply be due to the fact that the local heating is lessened by the moving beam front.

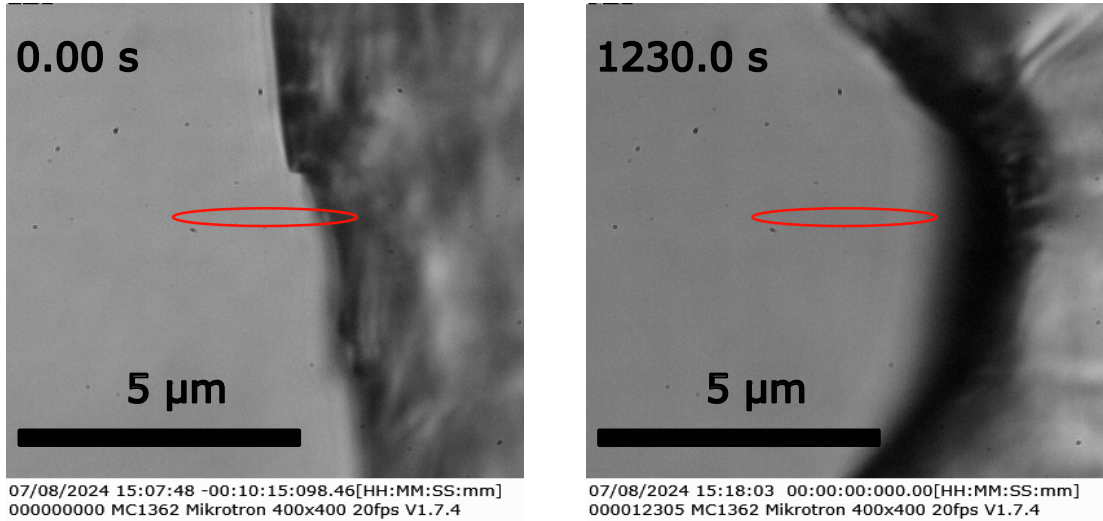


Figure 3.14: Frames from a seed crystal being irradiated by a scanning laser. The laser path is shown below in red. Initially the crystal edge is nearly perpendicular to the laser path. Over the course of nearly twenty minutes the crystal around the laser has dissolved leaving a concave indent.

3.6 Summary of Moving Beam Phenomena

To summarise, the introduction of a moving beam helps to accelerate the local growth of a newly formed crystal. It seems that this phenomena will only occur when close to interface between the solution and air. We note the presence of droplets that can sometimes be seen entering the trap, though this is not always necessary for a nucleation event to occur. A plausible description of the phenomena is described thusly.

Initial nucleation is similar to typical optical trapping induced nucleation, with the air solution interface limiting the molecular mobility of the solute molecules [21], [23], [30]. The moving beam front can influence the motion of the nucleus initially, but eventually the drag force means the crystal is not moved by the optical trap. Localised crystal growth occurs when the trap is close to or partially over the interface of the crystal (see fig. 3.15(a)). This suggests that the laser itself is bringing in new solute material that can then adhere to the crystal surface. Interestingly even when the crystal growth is localised to a small section of the crystal we do not observe the crystal dissolving. This is consistent with other observed laser induced nucleation results, where as long as the laser is active the crystal remains stable within the solution [21], [23]–[25]. It

does raise further questions however, mainly in an undersaturated solution is a moving beam front able to increase the size of the formed nucleus compared to a stationary beam? Additionally, it raises the question about what the role the 'glycine droplets' play in the nucleation process.

As shown in 3.5.3, the optical trap can manipulate these droplets similar to microspheres. When in close proximity to the trap these droplets are brought towards the crystal surface (see fig. 3.15(b)). We have already suggested that these droplets must contain glycine as they are to large to be a silica microsphere, and the solutions were filtered prior to being studied. The droplets provide material that grows the crystal around that region (see fig. 3.15(c)). Eventually the local solution is either depleted of solute material or the crystal front has grown to fully encompass the trap, preventing further growth (see fig. 3.15(d)).

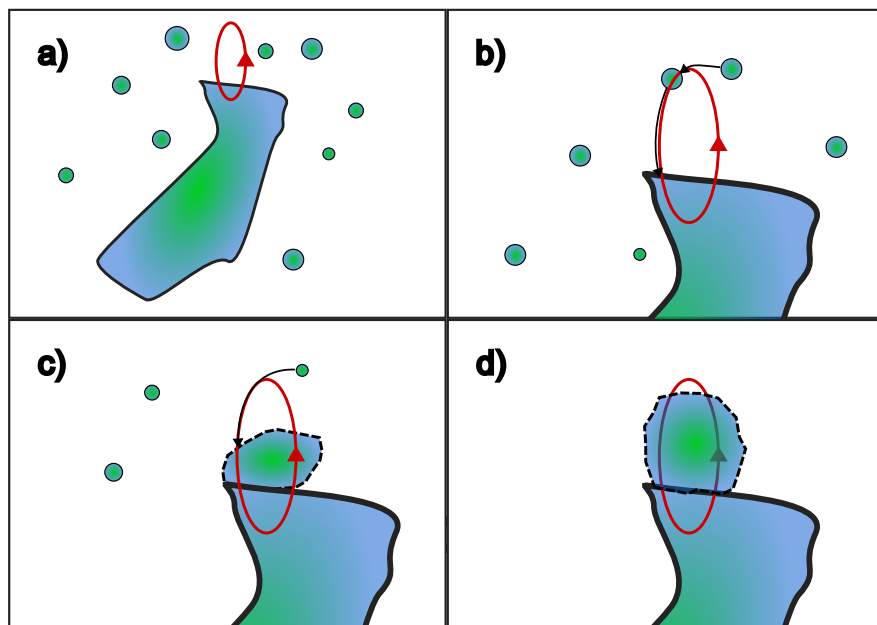


Figure 3.15: Diagram outlining how a moving beam assists in the growth of a crystal nucleus. (a) a crystal nucleus is partially trapped by a moving beam with solute droplets close to its surface. (b) droplets close to the laser focus can be drawn in by gradient forces and moved towards the crystal surface. (c) the laser brings in material that is then deposited on the surface of the crystal. (d) eventually the crystal area either fully surrounds the laser focus or the solution surrounding the laser is depleted of solute material.

What remains unclear is why the solution interface is necessary for localised crystal growth. We know that the glycine droplets will form when the laser is close to the glass-solution interface [22], [30], [33]. This is consistent with our results as being able to image the droplet edge requires that the laser is brought close to the cover slip. However it is not clear how exactly these droplets contribute to localised crystal growth as in sec. 3.5.2 no droplets are seen entering the trap. It seems likely that the presence of droplets is necessary as we see that the seed crystals dissolve while there are no droplets present.

There are still several factors that need to be investigated. Firstly, there is the question of what conditions result in the production of concentrated droplets, it is not clear if the presence of a laser is required or if these droplets naturally occurring. Prior literature would suggest that the laser is required [21], [29], but this would not explain why in many cases the droplets are found far outside the influence of the optical trap. It has been shown that phase separation occurs when a trap is focused close to the cover slip [22], [30], [33], but there has been no cases of nucleation occurring at the cover slip. Furthermore these experiments all occurred in supersaturated condition ($S \geq 1.50$) with a much wider focus ($NA \leq 1.00$) whereas our results occurred in undersaturated conditions with a tighter focus. We did not not any occurrence of a phase separation as reported by [22], [30], [33] and yet we see the appearance of droplets that we surmise are partially constructed of glycine.

Secondly, there is the question of how these droplets supply material to the bulk crystal. In some instances it is clear that the droplets are being drawn into the trap, however, in other instances while there are no droplets close to the vicinity of the optical trap the crystal continues to grow. If these droplets are a necessary precursor to induce crystal nucleation then understanding how they provide materials to the bulk crystal may help with our understanding of the kinetics of multi-step nucleation.

3.7 Conclusion

In conclusion, the experimental results from this chapter provide no affirmative evidence of shear induced crystal nucleation. This is in part due to the limited rotational speed that could be achieved using vaterite microspheres. Simply adding a micro-rotor to a supersaturated solution will not yield a significant fluid flow to induce crystal nucleation. Furthermore, the region in which the local shear rate is significant enough is so small that any nucleation events that could occur there may not grow large enough to be stable. This does not however, suggest that shear induced nucleation is impossible at a micro scale. In fact there have been several developments lately that allow for the precise rotation of multiple rotors to control the precise motion of silica beads [28]. This would allow for direct control of the shear rate within a given volume of fluid, allowing one to study the impact of fluid flow on a nucleus at a micro-scale.

On the other hand, the results utilising the galvano mirror have some interesting implications for future research into crystal nucleation using optical tweezers. We noted that a moving beam front is capable of localising the crystal growth around the beam focus in undersaturated conditions. Typically in laser induced nucleation the final crystal morphology is influenced primarily by the local fluid conditions [21], [24]. If this phenomena could be fully understood we could have a means of directly manipulating the morphology of any nucleating crystal. We noted that in undersaturated conditions the presence of droplets that could be trapped and later nucleated when brought into contact with one another. There remains some uncertainty over the role these droplets play in a nucleation event. Further research is also necessary to understand how the fluid and laser parameters (i.e. supersaturation and numerical aperture) impact the formation of these droplets. The fact that these droplets could be trapped suggests they have a higher refractive index to the solution, given that the solutions were filtered prior to irradiation dismisses that they could be dust particles. Prior literature suggests that optical trapping of a supersaturated solution can lead to the production of nano droplets [29], [30].

Bibliography

- [1] R. Debuyschère, B. Rimez, A. Zaccione, *et al.*, “Experimental and theoretical investigation of nonclassical shear-induced nucleation mechanism for small molecule,” *Crystal Growth & Design*, vol. 23, no. 7, pp. 4979–4989, Jun. 2023, ISSN: 1528-7505. DOI: [10.1021/acs.cgd.3c00232](https://doi.org/10.1021/acs.cgd.3c00232).
- [2] F. Mura and A. Zaccione, “Effects of shear flow on phase nucleation and crystallization,” *Physical Review E*, vol. 93, no. 4, p. 042803, Apr. 2016, ISSN: 2470-0053. DOI: [10.1103/physreve.93.042803](https://doi.org/10.1103/physreve.93.042803).
- [3] Y. Arita, J. M. Richards, M. Mazilu, *et al.*, “Rotational dynamics and heating of trapped nanovaterite particles,” *ACS Nano*, vol. 10, no. 12, pp. 11 505–11 510, Dec. 2016, ISSN: 1936-086X. DOI: [10.1021/acsnano.6b07290](https://doi.org/10.1021/acsnano.6b07290).
- [4] K. Saito and Y. Kimura, “Optically driven liquid crystal droplet rotator,” *Scientific Reports*, vol. 12, no. 1, Oct. 2022, ISSN: 2045-2322. DOI: [10.1038/s41598-022-21146-y](https://doi.org/10.1038/s41598-022-21146-y).
- [5] S. J. Parkin, R. Vogel, M. Persson, *et al.*, “Highly birefringent vaterite microspheres: Production, characterization and applications for optical micromanipulation,” *Optics Express*, vol. 17, no. 24, p. 21944, Nov. 2009, ISSN: 1094-4087. DOI: [10.1364/oe.17.021944](https://doi.org/10.1364/oe.17.021944).
- [6] J. G. J. R. G.-S. A. M. I. P. Castillo, “Optical tweezers - fromn calibration to applications: A tutorial,” *Optics*, 2020. DOI: <https://doi.org/10.48550/arXiv.2004.05246>. [Online]. Available: <https://arxiv.org/abs/2004.05246>.

Bibliography

- [7] H.-I. Kim, I.-J. Joo, S.-H. Song, *et al.*, “Dependence of the optical trapping efficiency on the ratio of the beam radius-to-the aperture radius,” *Journal of the Korean Physical Society*, vol. 43, no. 3, p. 348, 2003.
- [8] S. N. S. Reihani, M. A. Charsooghi, H. R. Khalesifard, *et al.*, “Efficient in-depth trapping with an oil-immersion objective lens,” vol. 31, p. 766, 2006, ISSN: 0146-9592. DOI: [10.1364/ol.31.000766](https://doi.org/10.1364/ol.31.000766).
- [9] G. M. Gibson, J. Leach, S. Keen, *et al.*, “Measuring the accuracy of particle position and force in optical tweezers using high-speed video microscopy,” *Optics Express*, vol. 16, no. 19, p. 14561, Sep. 2008, ISSN: 1094-4087. DOI: [10.1364/oe.16.014561](https://doi.org/10.1364/oe.16.014561).
- [10] K. Berg-Sørensen and H. Flyvbjerg, “Power spectrum analysis for optical tweezers,” vol. 75, pp. 594–612, 2004, ISSN: 0034-6748. DOI: [10.1063/1.1645654](https://doi.org/10.1063/1.1645654).
- [11] D. Konopacka-Łyskawa, “Synthesis methods and favorable conditions for spherical vaterite precipitation: A review,” *Crystals*, vol. 9, no. 4, p. 223, Apr. 2019, ISSN: 2073-4352. DOI: [10.3390/cryst9040223](https://doi.org/10.3390/cryst9040223).
- [12] Yugesha, S. Bhattacharya, and S. Ananthamurthy, “Characterizing the rotation of non symmetric objects in an optical tweezer,” *Optics Communications*, vol. 285, no. 10–11, pp. 2530–2535, May 2012, ISSN: 0030-4018. DOI: [10.1016/j.optcom.2012.01.055](https://doi.org/10.1016/j.optcom.2012.01.055).
- [13] F. Monteiro, S. Ghosh, E. C. van Assendelft, *et al.*, “Optical rotation of levitated spheres in high vacuum,” *Physical Review A*, vol. 97, no. 5, p. 051802, May 2018, ISSN: 2469-9934. DOI: [10.1103/physreva.97.051802](https://doi.org/10.1103/physreva.97.051802).
- [14] G. Volpe, O. M. Maragò, H. Rubinsztein-Dunlop, *et al.*, “Roadmap for optical tweezers,” *Journal of Physics: Photonics*, vol. 5, no. 2, p. 022501, Apr. 2023, ISSN: 2515-7647. DOI: [10.1088/2515-7647/acb57b](https://doi.org/10.1088/2515-7647/acb57b).
- [15] J. Millen, T. Deesawan, P. Barker, *et al.*, “Nanoscale temperature measurements using non-equilibrium brownian dynamics of a levitated nanosphere,” *Nature Nanotechnology*, vol. 9, no. 6, pp. 425–429, May 2014, ISSN: 1748-3395. DOI: [10.1038/nnano.2014.82](https://doi.org/10.1038/nnano.2014.82).

Bibliography

- [16] P. Rodríguez-Sevilla, Y. Arita, X. Liu, *et al.*, “The temperature of an optically trapped, rotating microparticle,” *ACS Photonics*, vol. 5, no. 9, pp. 3772–3778, Aug. 2018, ISSN: 2330-4022. DOI: [10.1021/acspophotonics.8b00822](https://doi.org/10.1021/acspophotonics.8b00822).
- [17] G. Knöner, S. Parkin, N. R. Heckenberg, *et al.*, “Characterization of optically driven fluid stress fields with optical tweezers,” *Physical Review E*, vol. 72, no. 3, p. 031507, Sep. 2005, ISSN: 1550-2376. DOI: [10.1103/physreve.72.031507](https://doi.org/10.1103/physreve.72.031507).
- [18] R. M. Robertson-Anderson, “Optical tweezers microrheology: From the basics to advanced techniques and applications,” *ACS Macro Letters*, vol. 7, no. 8, pp. 968–975, Aug. 2018, ISSN: 2161-1653. DOI: [10.1021/acsmacrolett.8b00498](https://doi.org/10.1021/acsmacrolett.8b00498).
- [19] G. D. Bruce, P. Rodríguez-Sevilla, and K. Dholakia, “Initiating revolutions for optical manipulation: The origins and applications of rotational dynamics of trapped particles,” *Advances in Physics: X*, vol. 6, no. 1, Dec. 2020, ISSN: 2374-6149. DOI: [10.1080/23746149.2020.1838322](https://doi.org/10.1080/23746149.2020.1838322).
- [20] A. I. Bishop, T. A. Nieminen, N. R. Heckenberg, *et al.*, “Optical microrheology using rotating laser-trapped particles,” *Physical Review Letters*, vol. 92, no. 19, p. 198 104, May 2004, ISSN: 1079-7114. DOI: [10.1103/physrevlett.92.198104](https://doi.org/10.1103/physrevlett.92.198104).
- [21] Z. Liao and K. Wynne, “A metastable amorphous intermediate is responsible for laser-induced nucleation of glycine,” vol. 144, pp. 6727–6733, 2022, ISSN: 0002-7863. DOI: [10.1021/jacs.1c11154](https://doi.org/10.1021/jacs.1c11154).
- [22] K.-i. Yuyama, T. Sugiyama, and H. Masuhara, “Millimeter-scale dense liquid droplet formation and crystallization in glycine solution induced by photon pressure,” *The Journal of Physical Chemistry Letters*, vol. 1, no. 9, pp. 1321–1325, Apr. 2010, ISSN: 1948-7185. DOI: [10.1021/jz100266t](https://doi.org/10.1021/jz100266t).
- [23] T. Sugiyama, T. Adachi, and H. Masuhara, “Crystal growth of glycine controlled by a focused cw near-infrared laser beam,” *Chemistry Letters*, vol. 38, no. 5, pp. 482–483, Apr. 2009, ISSN: 1348-0715. DOI: [10.1246/cl.2009.482](https://doi.org/10.1246/cl.2009.482).
- [24] J. Flannigan, “Optical tweezer and particle control of nucleation and growth at the microscale,” Ph.D. dissertation, University of Strathclyde, 2023. [Online].

Bibliography

- Available: <https://pureportal.strath.ac.uk/en/studentTheses/optical-tweezer-and-particle-control-of-nucleation-and-growth-at->.
- [25] T. Rungsimanon, K.-i. Yuyama, T. Sugiyama, *et al.*, “Crystallization in unsaturated glycine/d₂o solution achieved by irradiating a focused continuous wave near infrared laser,” vol. 10, pp. 4686–4688, 2010, ISSN: 1528-7483. DOI: 10.1021/cg100830x.
 - [26] T. Sugiyama and S.-F. Wang, “Manipulation of nucleation and polymorphism by laser irradiation,” *Journal of Photochemistry and Photobiology C: Photochemistry Reviews*, vol. 52, p. 100530, Sep. 2022, ISSN: 1389-5567. DOI: 10.1016/j.jphotochemrev.2022.100530.
 - [27] P. Patyar, K. Kaur, and G. Singh, “Viscometric and spectroscopic studies on interactions of glycine with aqueous buffer solutions,” *Journal of Molecular Liquids*, vol. 307, p. 112921, Jun. 2020, ISSN: 0167-7322. DOI: 10.1016/j.molliq.2020.112921.
 - [28] U. G. Butaitė, G. M. Gibson, Y.-L. D. Ho, *et al.*, “Indirect optical trapping using light driven micro-rotors for reconfigurable hydrodynamic manipulation,” *Nature Communications*, vol. 10, no. 1, Mar. 2019, ISSN: 2041-1723. DOI: 10.1038/s41467-019-08968-7.
 - [29] Y. Tsuboi, T. Shoji, and N. Kitamura, “Optical trapping of amino acids in aqueous solutions,” *The Journal of Physical Chemistry C*, vol. 114, no. 12, pp. 5589–5593, Dec. 2009, ISSN: 1932-7455. DOI: 10.1021/jp9072334.
 - [30] O. Y. Gowayed, T. Moosa, A. M. Moratos, *et al.*, “Dynamic light scattering study of a laser-induced phase-separated droplet of aqueous glycine,” vol. 125, pp. 7828–7839, 2021, ISSN: 1520-6106. DOI: 10.1021/acs.jpcb.1c02620.
 - [31] W. H. Orttung, “Polarizability and apparent radius of glycine from refractive index data,” *The Journal of Physical Chemistry*, vol. 67, no. 5, pp. 1102–1105, 1963, ISSN: 0022-3654. DOI: 10.1021/j100799a040.

Bibliography

- [32] E. J. Peterman, F. Gittes, and C. F. Schmidt, “Laser-induced heating in optical traps,” *Biophysical Journal*, vol. 84, no. 2, pp. 1308–1316, Feb. 2003, ISSN: 0006-3495. DOI: [10.1016/s0006-3495\(03\)74946-7](https://doi.org/10.1016/s0006-3495(03)74946-7).
- [33] K.-i. Yuyama, T. Rungsimanon, T. Sugiyama, *et al.*, “Formation, dissolution, and transfer dynamics of a millimeter-scale thin liquid droplet in glycine solution by laser trapping,” *The Journal of Physical Chemistry C*, vol. 116, no. 12, pp. 6809–6816, Mar. 2012, ISSN: 1932-7455. DOI: [10.1021/jp210576k](https://doi.org/10.1021/jp210576k).
- [34] P.-W. Yi, W.-H. Chiu, T. Kudo, *et al.*, “Cooperative optical trapping of polystyrene microparticle and protein forming a submillimeter linear assembly of microparticle,” *The Journal of Physical Chemistry C*, vol. 125, no. 34, pp. 18 988–18 999, Aug. 2021, ISSN: 1932-7455. DOI: [10.1021/acs.jpcc.1c05796](https://doi.org/10.1021/acs.jpcc.1c05796).